2D Materials

PAPER

Substrate, a choice of engineering the pseudospin in graphene

To cite this article: Jiahao Yan *et al* 2019 *2D Mater.* **6** 045050

2D Materials

RECEIVED
9 May 2019

REVISED
15 August 2019

ACCEPTED FOR PUBLICATION
4 September 2019

PUBLISHED
23 September 2019

PAPER

Substrate, a choice of engineering the pseudospin in graphene

Jiahao Yan[1,2], Liangmei Wu[1,2], Rui-Song Ma[1,2], Shiyu Zhu[1,2], Ce Bian[1,2], Jiajun Ma[1,2], Qing Huan[1,3,4], Lihong Bao[1,3,4,5], Jinhai Mao[2,5], Shixuan Du[1,3,4] and Hong-Jun Gao[1,2,3,4]

[1] Institute of Physics, Chinese Academy of Sciences, PO Box 603, Beijing 100190, People's Republic of China
[2] School of Physical Sciences, University of Chinese Academy of Sciences, Beijing 100190, People's Republic of China
[3] CAS Center for Excellence in Topological Quantum Computation, Beijing 100190, People's Republic of China
[4] Songshan Lake Materials Laboratory, Dongguan, Guangdong 523803, People's Republic of China
[5] Authors to whom any correspondence should be addressed.

E-mail: lhbao@iphy.ac.cn and jhmao@ucas.edu.cn

Keywords: pseudospin, corrugation, strain, graphene, GaSe

Supplementary material for this article is available online

Abstract

Structure and symmetry of crystal dictate their physical properties. Reasonable manipulation of those parameters allows designing the materials' properties in a nonchemical way, like the strain or pressure. Here we report the possibility of manipulating the pseudospin and lifting its degeneracy through the substrate corrugation in graphene, which directly relates to the chirality of Dirac fermions in the low energy regime. By a detailed scanning tunneling microscopy (STM) study that combined with van der Waals heterostructure fabrications, we find the pseudospin degeneracy can be continually lifted that materialized as the gradual wavefunction polarization on the two sublattices by changing graphene's curvature through a bump. Strikingly, the sublattice polarization shows a linear dependence on the geometry of bumps, which enables to extract a pseudo-*g*-factor to characterize the pseudospin splitting and geometry. Our results may shine light on engineering the pseudospin, the new degree of freedom, by a mechanical path.

Introduction

Graphene consists of a layer of carbon atoms forming a honeycomb pattern, where a unit cell contains a pair of sublattices, denoted as A and B [1]. To describe the orbital wavefunctions sitting in the two different sublattices, an extra degree of freedom that termed as pseudospin is introduced. Near the charge neutrality point, so-called Dirac point, the electronic features of carriers are described by the low energy relativistic physics but with spin replaced by pseudospin [2–5]. The direction of motion coupled to this pseudospin orientation endows the carriers in graphene a property, i.e. chirality, which has important consequences for transport, as manifested by the half-integer quantum Hall effect [2] and Klein tunneling [6]. Manipulating the pseudospin in graphene with a non-chemical method has aroused a great research interest both experimentally and theoretically in order to harness those Dirac fermions.

An intriguing proposal to control the pseudospin in graphene is to distort carbon–carbon (C–C) bonds by either the strain or the curvature [4, 7–13]. This bond deformation will introduce an effective gauge field [14] that have shown its potential to control the pseudospin polarization, and inspired the study of quantum valley Hall effect [15–17], valleytronics [18, 19] or even the magnetic confinement states [20]. Even though graphene possesses a strong in-plane Young's modulus owing to the carbon–carbon covalence bonds, it subjects to the out of plane deformation easily when it is put on a substrate with corrugation, a result of the competition between adhesion energy and bending energy. This allows graphene to coat the substrate surface and copy its features even though not exactly, and provides a strategy for engineering the topography through curvature. Here we perform a systematical study on manipulating the pseudospin in graphene lattice through a curvature effect by stacking it on different host substrates with various corrugation, which enable us to portray a possibility of manipulating pseudospin with the choice of environment or even mechanically like buckling in the thin membranes.

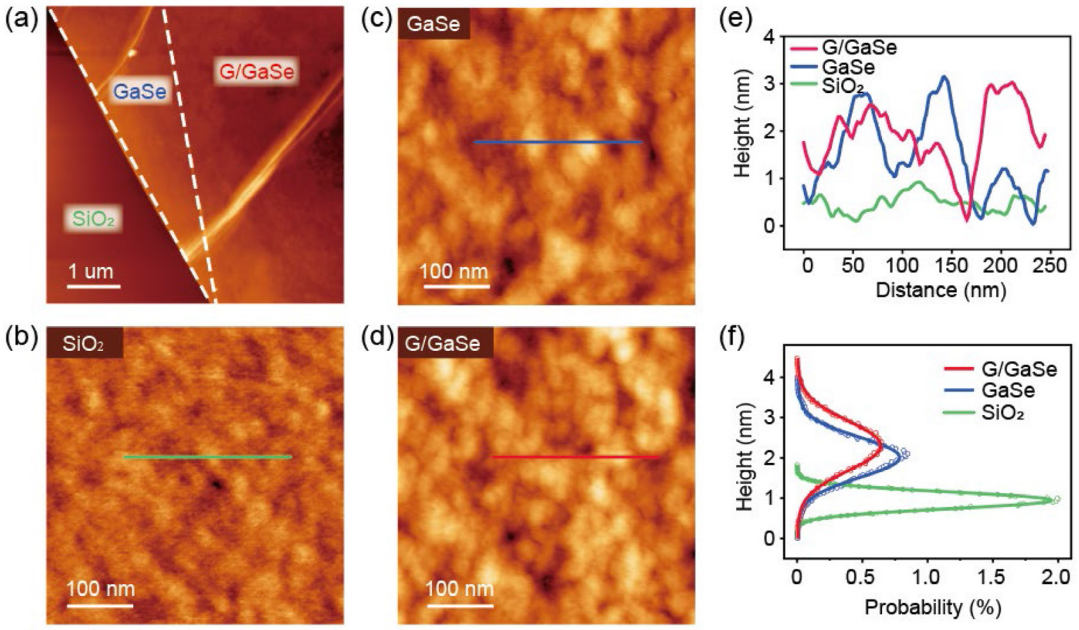

Figure 1. AFM morphology comparison of three types of surfaces. (a) AFM morphologic image shows three different areas, SiO_2, GaSe and G/GaSe, divided by the dashed lines. (b)–(d) Detailed AFM images show the roughness of three different kind of surfaces in (a), representing surfaces of SiO_2 (b), GaSe (c) and G/GaSe (d). (e) Height profiles of three surfaces along solid lines in (b), (c) and (d), respectively. (f) Height histograms reveal height distribution of SiO_2, GaSe and G/GaSe surfaces (discrete circular points) acquired from entire range in (b)–(d), respectively. These histograms are well fitted by Gaussian distributions (solid lines).

Results and discussion

Figure 1(a) shows a typical atomic force microscopy (AFM) image of the heterostructure fabricated in glove box by placing graphene on multilayer gallium selenide (G/GaSe) which is finally placed on the SiO_2 substrate (figure 2(a)). During the transferring graphene process, we use Ar gas in glove box to protect the GaSe surface from any pollution and confirm the clean interference between graphene and GaSe underneath. Zoom-in AFM topography of silicon dioxide (SiO_2) in figure 1(b) and GaSe in figure 1(c) directly reveals GaSe has a much larger fluctuation in range (~3 nm) than SiO_2 surface (~1 nm) (figure 1(e)) which provide a prerequisite for engineering graphene through the curvature. After stacking graphene on top (figure 1(d)), the topography of G/GaSe (red line in figure 1(e)) shows a height profile that is similar to bare GaSe surface (blue line in figure 1(e)). In addition, the height histograms of these three surfaces, which all fit the Gaussian distributions well, has the same features that G/GaSe has a similar distribution curve (red line in figure 1(f)) to bare GaSe surface (blue line in figure 1(f)) and is much broader distributed than SiO_2 surface (green line in figure 1(f)). The cleanness of the SiO_2 surface and typical corrugation [21] directly excludes the residues caused roughness on top of graphene in figure 1(d), but a simple copy for the substrate morphology. Here, GaSe surface shows a larger surface corrugation as compared to the normal exfoliated van der Waals materials, which may due to the chemical reaction with the air during the sample fabrication [22–25] or in the forming gas with H_2. However, since the mechanism has no bearing on the physics discussed below, we will leave this question open and employ the large corrugated substrate only to regulate the pseudospin.

In order to relate the curvature or bond deformation in graphene to the pseudospin manipulation, we directly examine atomic structure by scanning tunneling microscopy (STM), where the pseudospin degeneracy manipulation materialize as the A and B atoms contrast difference. Figure 2(d) shows our STM topography of G/GaSe with a typical height fluctuation around 3 nm in range (figure 2(f)) that is consistent with the AFM results in figure 1, suggesting the morphology dominates the STM topography instead of the electronic features like electron-hole puddles. Strikingly, the atomic resolution for this area shows a triangular lattice (figure 2(g)) instead of the as expected honeycomb pattern in intrinsic graphene. To exclude the misidentification between single and multilayer graphene, the Raman spectrum is utilized to further confirm graphene's single layer character (figure S1 (stacks.iop.org/TDM/6/045050/mmedia)). As far as we know, three mechanisms can lead to the sublattice symmetry breaking: (1) graphene hybridized with the substrates [26]; (2) electronic structure reconstruction like in the nanoribbons [27] or near the defects; (3) the curvature or strain effect as caused by the corrugation. However, due to the large misaligned twisted angle between the two layers during stacking, lattice constant mismatch and large corrugation of the GaSe, an exact atomic registry between graphene

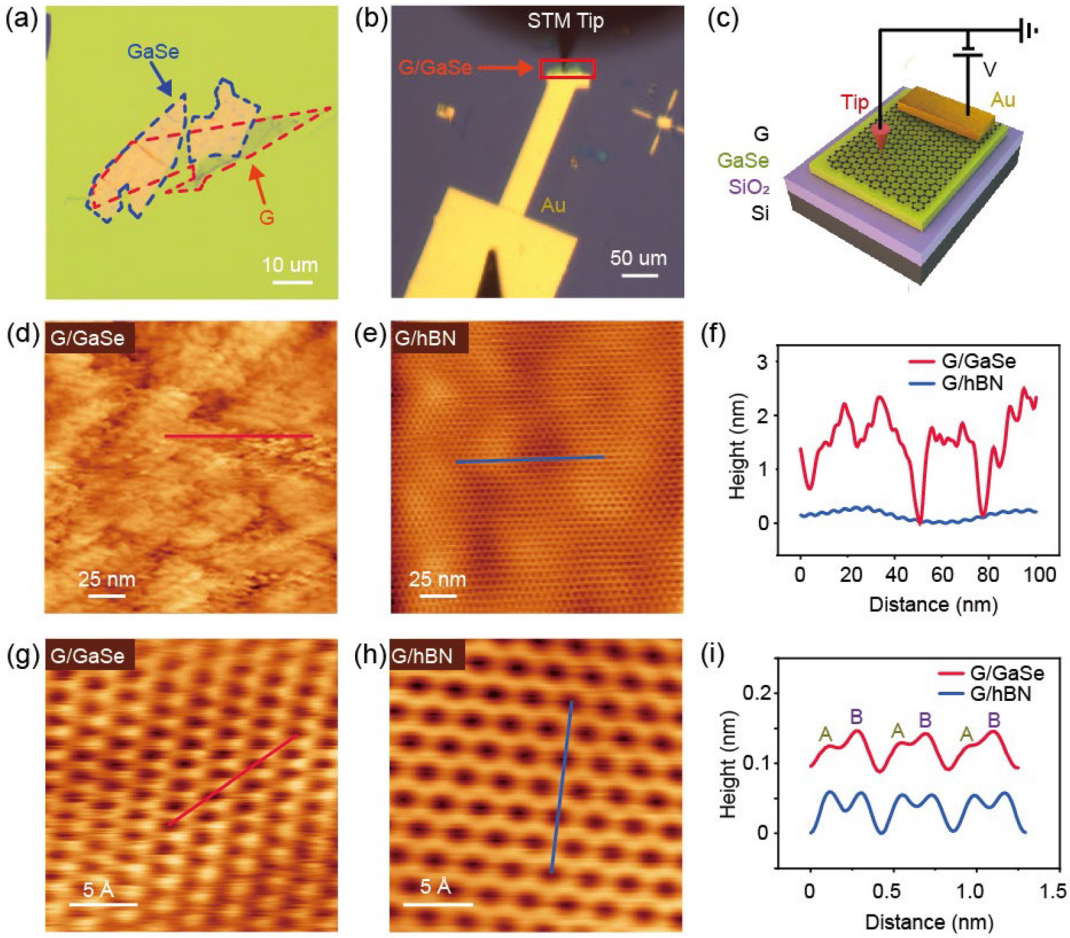

Figure 2. Fabrication process and STM topography of sampls. (a) Optical image G/GaSe heterostructure after transferring G (red dashed line) on GaSe flake (blue dashed line) in glove box. (b) Optical image of G/GaSe device (red square box) with evaporated Au electrode during STM experiment. (c) Schematic drawing of STM experiment. (d) and (e) Large scale STM topography of G/GaSe (d) and G/BN (e) respectively ($V = 0.5$ V, $I = 100$ pA). (f) Height profile comparison between G/GaSe and G/BN obtained along red line (d) and blue line (e). (g) and (h) Atomic resolution of G/GaSe shows triangular lattice (g), but that of G/BN shows intrinsic honeycomb structure (h). Tunneling parameters: $V = 0.5$ V, $I = 500$ pA (g); $V = 0.3$ V, $I = 100$ pA (h). (i) Height profiles show the contrast between two sublattices (marked as A and B) of G/GaSe and G/BN along one of the armchair direction along red line (g) and blue line (h). The curves are offset for clarity.

and GaSe to induce the sublattice symmetry can be excluded. The scanned area is far away from any edge or defect, especially its universal behavior of the triangular lattice across the whole sample areas, also exclude the possibility of electronic states reconstruction due to edge. Therefore, taking all those into account, and in addition to the large corrugation as indicated by the AFM and STM images, our data suggest the triangular lattices are caused by the corrugation.

As graphene subjects to curvature or external strain, the lattices deforms which modifies the hopping parameter as the relative atoms' distance variation [14]. This will introduce a vector potential in the Hamiltonian that describe the low energy excitation of graphene. Interestingly, this strain-induced vector potential resembles the corresponding vector potential by external magnetic field. It enables to reshape the energy dispersion of graphene or topological crystalline insulator, given the so-called pseudomagnetic field or even pseudo-Landau levels [7, 28] where the amplitude of the pseudomagnetic field value is uniform within the magnetic length. The strain induced gauge field is capable of allowing the wave functions to polarize on different sublattice depending on its polarity. Even though the relative scale of magnetic length as comparing to the homogeneity of strain or curvature decides whether the pseudo-Landau levels to show up, the wave function polarization between the two sublattices is ubiquitous signature under strain or curvature. This explains why we could see the triangular lattices here instead of honeycomb in graphene.

As a control experiment, we also compared graphene on boron nitride (G/BN) that fabricated by following the same procedure but resulting in a smoother surface (figure 2(e)). Similar to our previous experimental STM results, the atomic resolution here shows a honeycomb structure in figure 2(h), where A and B sublattice have identical height compared with G/GaSe (figure 2(i)). The healing of sublattice symmetry in the flat sample surface, here G/BN, further proves the importance of the corrugation on deciding the sublattice symmetry, providing a way to engineer the

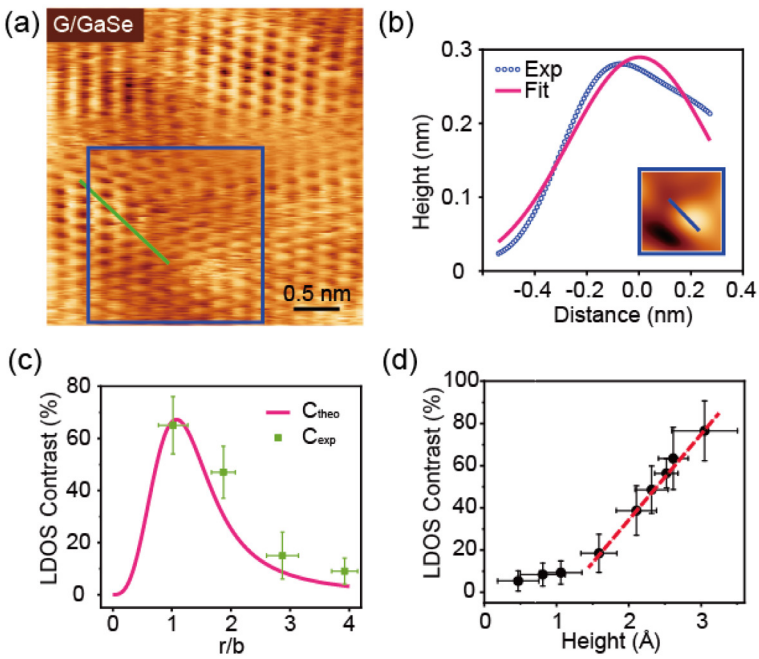

Figure 3. Relating sublattice symmetry breaking to substrate morphology corrugation. (a) Atomic resolution image of G/GaSe also obtained in figure 2(d). Tunneling parameters: $V = 0.5$ V, $I = 500$ pA. (b) Height profile of the bump in the inset. Pink curve is the Gaussian fitting. Inset: substrate corrugation deduced by low-pass FFT from the area marked by a blue solid square in (a). (c) The plot of LDOS contrast as a function of r/b. r is the distance from the bump's center in (a) and b is the width of Gaussian deformation. Experimental data are obtained from (a) and (b) and the pink curve is the theoretical calculation. (d) The plot of the LDOS contrast as a function of the height of the substrate. The discrete black points with error bars are experimental results and the red dashed line is guide for the eye to reveal the linear relationship with larger height.

pseudospin freedom by the buckling that could be realized mechanically.

Now we use the following theoretical model [4, 12] to explain sublattice symmetry breaking of graphene. A Gaussian shaped deformation in graphene honeycomb lattice could induce pseudomagnetic field and cause the sublattice symmetry breaking which means that the LDOS redistribute between the two sublattices exhibiting a triangular lattice, compared with undeformed case exhibiting a honeycomb lattice observed in STM experiment. Since we care about the occupation of LDOS between different sublattices, the universal definition of LDOS contrast is $C = 2\frac{|\nu_A - \nu_B|}{\nu_A + \nu_B}$ [12], where $\nu_{A/B}$ is the sublattice resolved LDOS of sublattice A/B, which is a quantity of experimental relevance. Specially, the spatial distribution of LDOS contrast in Gaussian shape deformed graphene was theoretically obtained by the formula:

$$C_{\text{theo}}(r,\theta) = -\frac{2\beta H^2}{ba}\sin(3\theta)\, g(r/b) \qquad (1)$$

($g(x) = \frac{1}{4x^3}[1 - e^{-2x^2}(1 + 2x^2 + 2x^4)]$, where θ is the azimuthal angle, r is the distance from center, $\beta = 3$, a is the lattice constant of graphene, H is the height of the Gaussian bump, and b is the width of the Gaussian deformation). To keep the analysis simple but without loss of generality, we assume the corrugations in graphene induced by the substrate possess a Gaussian shape as suggested in figure 3(a). The low-pass FFT filtering operation is implemented on the area marked by the blue square in figure 3(a) to acquire the topography of the bump (Inset in figure 3(b)). And the height profile along the blue line of the bump (Inset in figure 3(b)) is shown in figure 3(b) with discrete blue circles which is fitted by the equation $z(r) = H\exp(-x^2/b^2)$ shown in figure 3(b) with pink curve to extract H (0.29 nm) and b (0.4 nm). Then, with extracted parameter H and b, the theoretical LDOS contrast (pink curve with legend C_{theo} in figure 3(c)) as a function of r/b was calculated using the $C_{\text{theo}}(r,\theta)$ formula above at a fixed angle θ (90°) which has the maxim value. To compare with our results, we determine the experimental LDOS contrast C_{exp} by [4]

$$C_{\text{exp}} = 2\frac{e^{K\Delta z} - 1}{e^{K\Delta z} + 1} \qquad (2)$$

with $K = \sqrt{\frac{8m_e}{\hbar^2}\left(\frac{\Phi_G + \Phi_W}{2} - \frac{e|V|}{2}\right)}$, m_e is the free electron mass, V is the sample voltage and $\Delta z = |Z_A - Z_B|$ directly measure from the high-pass FFT filtered STM topography of figure 3(a) along the green line which includes four pairs of A/B sublattice points and the experimental results plotted with four discrete green points in figure 3(c) qualitatively and quantitatively fits the theoretical curve which confirms the sublattice symmetry in graphene as caused by the corrugation.

With those understanding in mind, we next study the relation of sublattice symmetry (also termed as pseudospin degeneracy) to the corrugation, which

would serve as a calibration table on further tuning the pseudospin. Figure 3(d) shows the evolution of LDOS contrast with the height of Gaussian bumps H at fixed bump width b and distance from the center (figure S2 for details). The monotonically decreasing of LDOS contrast with H indicates that the corrugation provides a useful knob on tuning the degeneracy of the pseudospin. Interestingly, for the height value becomes larger than 1.5 Å, the LDOS contrast value shows an almost linear dependence on the height, i.e. $C_{\mathrm{exp}} = g_{\mathrm{P}}H$, where the $g_{\mathrm{P}} = 0.4\,\mathring{\mathrm{A}}^{-1}$ is a prefactor that characterize the pseudospin splitting and the height that controls the curvature. This is reminiscent of Zeeman splitting as the spin degenerated states under an external magnetic field. However, the pseudospin degeneracy here is lifted by the curvature or height of the bump in our experiment. While it is worth to notice that this simple projection comes from a statistical result, i.e. the linear dependence of the LDOS contrast on the height of the bump, whether it could represent a universal case in the curved sample may still need further experimental work especially considering their nontrivial relationship as stated by equation (1).

Conclusion

In conclusion, we observed the sublattice symmetry breaking in graphene on GaSe substrate by STM. Topographic images of graphene reveal a triangular lattice with three-fold symmetry rather than intrinsic honeycomb lattice with six-fold symmetry when it is placed on a GaSe substrate. It is further confirmed by AFM that the corrugation of graphene on GaSe is caused by the large fluctuation and corrugation of topography in GaSe substrate (~3 nm), which is much larger than SiO_2 substrate (~1 nm). Experimental LDOS contrast between two sublattices of graphene according to height measured by STM is consistent with theoretical simulations. Our results provide a way to engineer the pseudospin or related electronic structure through a mechanical knob.

Methods

The G/GaSe heterostructure was fabricated in the glove box transferring multilayer exfoliated GaSe flake on the SiO_2 substrate followed by placing single layer graphene upon it (figure 2(a)). Then Au electrode connected with graphene sheet to supply bias voltage during STM imaging was defined by standard electron-beam lithography patterning followed by electron-beam evaporation Ti/Au (5/50 nm) and lift off. To remove PMMA residues, the device was annealed both in flowing H_2/Ar gas at 250 °C and in ultra-high vacuum at 250 °C for overnight. With a home-upgraded UHV four-probe scanning tunneling microscope [29], one of the tip made of gold contact with the electrode pad to supply bias voltage and another tip made of tungsten characterize the topography of the graphene sheet on GaSe (figures 2(b) and (c)). For the G/BN heterostructure, it follows the same process.

Acknowledgments

This work was supported by the grants from National Key Research & Development Projects of China (Nos. 2016YFA0202300 and 2018FYA0305800), National Natural Science Foundation of China (Nos. 61674170, and 61888102), the Strategic Priority Research Program of Chinese Academy of Sciences (Nos. XDB30000000) and Youth Innovation Promotion Association of CAS (20150005). J.M. is also supported by the University of Chinese Academy of Sciences.

ORCID iDs

Jiahao Yan https://orcid.org/0000-0002-3333-0669
Rui-Song Ma https://orcid.org/0000-0002-9954-4416
Shiyu Zhu https://orcid.org/0000-0002-8771-5273
Lihong Bao https://orcid.org/0000-0002-2942-892X
Hong-Jun Gao https://orcid.org/0000-0002-6766-0623

References

[1] Castro Neto A H, Guinea F, Peres N M R, Novoselov K S and Geim A K 2009 The electronic properties of graphene *Rev. Mod. Phys.* **81** 109–62
[2] Novoselov K S, Geim A K, Morozov S V, Jiang D, Katsnelson M I, Grigorieva I V, Dubonos S V and Firsov A A 2005 Two-dimensional gas of massless Dirac fermions in graphene *Nature* **438** 197–200
[3] Sasaki K, Wakabayashi K and Enoki T 2010 Polarization dependence of Raman spectra in strained graphene *Phys. Rev.* B **82** 205407
[4] Georgi A *et al* 2017 Tuning the pseudospin polarization of graphene by a pseudomagnetic field *Nano Lett.* **17** 2240–5
[5] Van Duppen B and Peeters F M 2013 Four-band tunneling in bilayer graphene *Phys. Rev.* B **87** 205427
[6] Katsnelson M I, Novoselov K S and Geim A K 2006 Chiral tunnelling and the Klein paradox in graphene *Nat. Phys.* **2** 620–5
[7] Guinea F, Katsnelson M I and Geim A K 2010 Energy gaps and a zero-field quantum Hall effect in graphene by strain engineering *Nat. Phys.* **6** 30–3
[8] Moldovan D, Masir M R and Peeters F M 2013 Electronic states in a graphene flake strained by a Gaussian bump *Phys. Rev.* B **88** 035446
[9] Neek-Amal M, Covaci L, Shakouri K and Peeters F M 2013 Electronic structure of a hexagonal graphene flake subjected to triaxial stress *Phys. Rev.* B **88** 115428
[10] Carrillo-Bastos R, Faria D, Latge A, Mireles F and Sandler N 2014 Gaussian deformations in graphene ribbons: flowers and confinement *Phys. Rev.* B **90** 041411
[11] Sanjuan A A P, Wang Z F, Imani H P, Vanevic M and Barraza-Lopez S 2014 Graphene's morphology and electronic properties from discrete differential geometry *Phys. Rev.* B **89** 121403
[12] Schneider M, Faria D, Kusminskiy S V and Sandler N 2015 Local sublattice symmetry breaking for graphene with a centrosymmetric deformation *Phys. Rev.* B **91** 161407

[13] Settnes M, Power S R and Jauho A P 2016 Pseudomagnetic fields and triaxial strain in graphene *Phys. Rev.* B **93** 035456
[14] Pereira V M and Castro Neto A H 2009 Strain engineering of graphene's electronic structure *Phys. Rev. Lett.* **103** 046801
[15] Marino E C, Nascimento L O, Alves V S and Smith C M 2015 Interaction induced quantum valley Hall effect in graphene *Phys. Rev.* X **5** 011040
[16] Ghaemi P, Ryu S and Lee D H 2010 Quantum valley Hall effect in proximity-induced superconducting graphene: an experimental window for deconfined quantum criticality *Phys. Rev.* B **81** 081403
[17] Islam S K F and Benjamin C 2016 A scheme to realize the quantum spin-valley Hall effect in monolayer graphene *Carbon* **110** 304–12
[18] Rycerz A, Tworzydlo J and Beenakker C W J 2007 Valley filter and valley valve in graphene *Nat. Phys.* **3** 172–5
[19] Garcia-Pomar J L, Cortijo A and Nieto-Vesperinas M 2008 Fully valley-polarized electron beams in graphene *Phys. Rev. Lett.* **100** 236801
[20] De Martino A, Dell'Anna L and Egger R 2007 Magnetic confinement of massless Dirac fermions in graphene *Phys. Rev. Lett.* **98** 066802
[21] Jiang Y, Lo P W, May D, Li G, Guo G Y, Anders F B, Taniguchi T, Watanabe K, Mao J and Andrei E Y 2018 Inducing Kondo screening of vacancy magnetic moments in graphene with gating and local curvature *Nat. Commun.* **9** 2349
[22] Drapak S I, Gavrylyuk S V, Kovalyuk Z D and Lytvyn O S 2008 Native oxide emerging of the cleavage surface of gallium selenide due to prolonged storage *Semiconductors* **42** 414–21
[23] Tan J Y *et al* 2014 Electronic transport in graphene-based heterostructures *Appl. Phys. Lett.* **104** 183504
[24] Andres-Penares D, Cros A, Martinez-Pastor J P and Sanchez-Royo J F 2017 Quantum size confinement in gallium selenide nanosheets: band gap tunability versus stability limitation *Nanotechnology* **28** 175701
[25] Shi L, Li Q, Ouyang Y X and Wang J L 2018 Effect of illumination and Se vacancies on fast oxidation of ultrathin gallium selenide *Nanoscale* **10** 12180–6
[26] Liu Y P *et al* 2018 Tailoring sample-wide pseudo-magnetic fields on a graphene-black phosphorus heterostructure *Nat. Nanotechnol.* **13** 828–34
[27] Jacobse P H, Kimouche A, Gebraad T, Ervasti M M, Thijssen M, Liljeroth P and Swart I 2017 Electronic components embedded in a single graphene nanoribbon *Nat. Commun.* **8** 119
[28] Levy N, Burke S A, Meaker K L, Panlasigui M, Zettl A, Guinea F, Neto A H C and Crommie M F 2010 Strain-induced pseudo-magnetic fields greater than 300 Tesla in graphene nanobubbles *Science* **329** 544–7
[29] Ma R S, Huan Q, Wu L M, Yan J H, Zou Q, Wang A W, Bobisch C A, Bao L H and Gao H J 2017 Upgrade of a commercial four-probe scanning tunneling microscopy system *Rev. Sci. Instrum.* **88** 063704